JOURNAL OF MAGNETIC RESONANCE **126,** 79–86 (1997)
ARTICLE NO. MN971145

NMR of Laser-Polarized ^{129}Xe in Blood Foam

C. H. Tseng,*,† S. Peled,*,‡ L. Nascimben,* E. Oteiza,† R. L. Walsworth,† and F. A. Jolesz *

*Brigham and Women's Hospital and Harvard Medical School, 221 Longwood Ave., Boston, Massachusetts 02115; †Smithsonian Astrophysical Observatory, Cambridge, Massachusetts 02138; and ‡Massachusetts Institute of Technology, Cambridge, Massachusetts 02139

Received October 15, 1996; revised February 10, 1997

Laser-polarized ^{129}Xe dissolved in a foam preparation of fresh human blood was investigated. The NMR signal of ^{129}Xe dissolved in blood was enhanced by creating a foam in which the dissolved ^{129}Xe exchanged with a large reservoir of gaseous laser-polarized ^{129}Xe. The dissolved ^{129}Xe T_1 in this system was found to be significantly shorter in oxygenated blood than in deoxygenated blood. The T_1 of ^{129}Xe dissolved in oxygenated blood foam was found to be approximately 21 ($\pm$5) s, and in deoxygenated blood foam to be greater than 40 s. To understand the oxygenation trend, T_1 measurements were also made on plasma and hemoglobin foam preparations. The measurement technique using a foam gas–liquid exchange interface may also be useful for studying foam coarsening and other liquid physical properties. © 1997 Academic Press

INTRODUCTION

Of the stable noble gas isotopes, only ^{3}He and ^{129}Xe have spin-$\frac{1}{2}$ nuclei which make them suitable for MRI. Optical pumping techniques (*1–3*) allow the spin polarization of these noble-gas nuclei far above thermal levels. Such large nuclear polarizations greatly enhance the NMR sensitivity of ^{129}Xe and ^{3}He, enabling a variety of applications in the physical sciences (*4, 5*), as well as in biomedical NMR (*6, 7*). Only ^{129}Xe is practical for tissue MRI because its solubility in tissue is much larger than that of ^{3}He (*8*). Laser-polarized ^{3}He (*9–11*) and ^{129}Xe (*12–14*) magnetic resonance images of animal and human lung gas spaces have been reported. *In vivo* ^{129}Xe tissue resonances have been observed in live mice (*13*), live rats (*12, 15*), and most recently in the human brain (*14*). The rodent resonances had decay times of ~10–50 seconds. A chemical-shift image of inhaled, laser-polarized ^{129}Xe in a live rat brain has also been obtained (*16*).

For laser-polarized ^{129}Xe NMR to be a useful tool for studies of perfused tissue, the ^{129}Xe spin polarization (or longitudinal) relaxation time, T_1, in arterial blood should be greater than the time it takes for inhaled ^{129}Xe to be transported to a particular tissue (typically 5–10 s in humans). The dependence of the concentration of polarized ^{129}Xe in various tissues on the T_1 in blood has been modeled in Ref. (*17*). A previous *in vitro* measurement of the T_1 of ^{129}Xe in blood found 4.5 $\pm$ 1 s in red blood cells and 9 $\pm$ 2 s in plasma (*18*). This experiment used thermally polarized ^{129}Xe and therefore required many hours of signal averaging. Potential systematic problems with such long measurement times include sedimentation and degradation of the blood.

In their recent demonstration of an injectable polarized ^{129}Xe agent, Bifone *et al.* (*19*) found a 5 s ^{129}Xe T_1 in blood using an open-air sample tube, which may have affected the value obtained. In the reported *in vivo* rodent investigations of polarized ^{129}Xe dissolved in blood and other tissues (*12, 13, 15*), only effective polarization lifetimes were determined because of the ^{129}Xe exchange with the lung gas space and other tissues. In contrast, the measurement reported here exploits the ^{129}Xe gas–blood phase exchange in a closed *in vitro* system. The surface area for exchange was delibrately increased by shaking the blood–gas sample to create a foam. Because the gas phase ^{129}Xe has a longer T_1 and greater density than the blood phase ^{129}Xe, the gas phase served as a source of ^{129}Xe magnetization. Thus, the foam system increased the amplitude and lengthened the observed lifetime of the NMR signal from ^{129}Xe dissolved in the blood. The ^{129}Xe exchange between the gas and blood phases was accounted for in the analysis of the observed decaying ^{129}Xe NMR signals. Because of the dependence of the exchange on the surface area, the ^{129}Xe signal may also be an indicator of foam-structure evolution such as coarsening or drainage.

THEORY

Let the ^{129}Xe magnetization in the gas phase be labeled G, and that dissolved in the blood phase B. Here and throughout this report, we use the term ''magnetization'' to describe the ensemble magnetic moment—an extensive variable. The ^{129}Xe NMR resonance frequencies of these phases are observed to be approximately 200 ppm apart which makes both separately measurable. The total number of xenon atoms is conserved in a closed system. The ^{129}Xe magnetization in each phase can change because of (a) exchange between the phases, (b) RF interrogation, or (c) T_1 relaxation of the spin polarization back to thermal equilibrium.

1090-7807/97 $25.00

From the relative initial signals of the ^{129}Xe gas- and blood-phase peaks and from the known solubility of xenon in blood (*8*), we determined that the xenon concentrations in the blood samples in our experimental system were approximately 2% of saturation. This low xenon concentration, and the observed speed with which the blood-phase signal was affected by RF pulses on the gas resonance, implies that all the ^{129}Xe blood signal came from the blood foam. Thus, we model the two-phase exchange system in the presence of a series of equally spaced RF pulses as (*20*)

$$\frac{dG}{dt} = -R'_G G - k_G G + k_B B \quad [1]$$

$$\frac{dB}{dt} = -R'_B B - k_B B + k_G G, \quad [2]$$

where $R'_G = R_G - (\ln \cos \theta_G)/\tau$ and $R'_B - (\ln \cos \theta_B)/\tau$. The logarithm terms are due to the effect of the RF read pulses spaced time τ apart with flip angles $\theta_{G,B}$ on the gas and blood, respectively. This effect can be derived by noting that the magnetization remaining at time $t = n\tau$, after n RF read pulses, is $G(t) = G_0(\cos \theta_G)^n$ assuming no exchange or T_1 relaxation. The constants, R_G and R_B, are the intrinsic longitudinal relaxation rates ($1/T_1$) of ^{129}Xe in the gas and the blood. The values of k_G and k_B are the xenon gas-to-blood and blood-to-gas chemical exchange rates. These constants can be interpreted as reciprocal residence times.

The solutions of Eqs. [1] and [2] are of biexponential form (*21*)

$$G = G_1 e^{-\mu_1 t} + G_2 e^{-\mu_2 t}, \quad [3]$$

$$B = B_1 e^{-\mu_1 t} + B_2 e^{-\mu_2 t}, \quad [4]$$

where

$$\mu_{1,2} = \frac{1}{2}\left[k_G + k_B + R'_G + R'_B \mp \sqrt{(k_G - k_B + R'_G - R'_B)^2 + 4k_G k_B}\right]. \quad [5]$$

The constants $G_{1,2}$ and $B_{1,2}$ depend on the initial conditions. Equations [3]–[5] describe well the measured signals in our experiments (see below).

For our system, the ^{129}Xe magnetization relaxation time in the gas phase is longer than in the dissolved phase, i.e., $R_G < R_B$, resulting also in $R'_G < R'_B$. This analysis will not be effective for cases in which this condition does not hold. Due to the much larger quantity of gas-phase xenon than dissolved blood-phase xenon, detailed balance implies that the xenon residence time in the gas ($\tau_G = 1/k_G$) is much longer than in the blood, i.e., $k_G \ll k_B$. Under these conditions,

$$\mu_1 = R'_B + k_B, \quad [6]$$

and from Eq. [2],

$$\frac{dB}{dt} = -\mu_1 B + k_G G. \quad [7]$$

Note two important limiting cases: (a) $G \gg B$, which results in $G \simeq G_2 e^{-\mu_2 t}$; and (b) $G \to 0$, e.g., after reduction of G with 90° pulses, which results in $B \simeq B_1 e^{-\mu_1 t}$.

The time behavior of the total magnetization, $G + B$, does not depend on the exchange rates, as can be seen by adding Eqs. [1] and [2]. R_B and R_G can be obtained if both $G(t)$ and $B(t)$ are known. In practice however, this approach cannot be effectively utilized because of sensitivity limitations. Therefore, to extract the pure T_1 value from the measured decay rate μ_1, the exchange rate, k_B, must be estimated. The lower bound for k_B is 0. Since the solubility of xenon in blood does not depend on the oxygenation level (*22*), an upper bound for k_B, using Eq. [6] and the definition of R'_B, is $\mu_{1(low)} + (\ln \cos \theta_B)/\tau$, where $\mu_{1(low)}$ is the lowest measured value of μ_1 for different oxygenations in a given sample type. These estimates permit only an upper bound for the deoxygenated decay rate, R_B. Limits on the blood-phase ^{129}Xe T_1 are expressed in Eq. [8]

$$\left(\mu_1 + \frac{\ln \cos \theta_B}{\tau}\right)^{-1} < T_1 < (\mu_1 - \mu_{1(low)})^{-1}. \quad [8]$$

The determination of the ^{129}Xe T_1 in the dissolved phase should not depend on the initial relative magnetizations of the blood and gas phases or on the relaxation rate in the gas phase. Experimental tests were consistent with the model described above—see Results.

MATERIALS AND METHODS

Preparation of the polarized-^{129}Xe gas sample followed procedures described elsewhere (*1, 23*). Angular momentum from circularly polarized light was transferred to electronic and then nuclear spins, through a process known as spin-exchange optical pumping, producing a nuclear-spin polarization far above thermal equilibrium (*24, 25*). In the experiments reported here, the ^{129}Xe nuclei were polarized to about 10% of complete alignment through spin-exchange collisions with optically pumped rubidium vapor (*1*). This 10% polarization should be compared to the thermal ^{129}Xe polarization of ~0.002% at 4.7 T. The xenon was contained in a 25 ml cylindrical Pyrex cell coated with OTS (octadecyltrichlorosilane) in order to reduce the effect of relaxation of

the ^{129}Xe polarization due to wall interactions. The Pyrex cell contained a few grams of rubidium metal of natural isotopic abundance, about 100 torr of N_2, and 3 atm of xenon gas of natural isotopic abundance (26% rich in the ^{129}Xe isotope). During the optical pumping phase, the cell was placed in the fringe field ($\sim$100 G) of the 4.7 T Bruker small animal MR imager in which the NMR experiments were performed. A hot air oven maintained the cell at about 100°C. Circularly polarized 795 nm light from two Ga–Al–As multistripe diode lasers (manufactured by Optopower, Inc.) optically pumped the $5^2S_{1/2}$ to $5^2P_{1/2}$ transition (the D1 spectral line) of the rubidium atoms creating an electron spin polarization. These atoms then polarized the nuclei of the ^{129}Xe atoms through spin-exchange collisions. After about 20 min, the cell was removed from the oven and laser beam and cooled to room temperature. The ^{129}Xe gas was cryopumped, using liquid nitrogen, into a second coated Pyrex cell with insignificant loss of ^{129}Xe polarization (*7*). When this cell was warmed back up to room temperature, the polarized ^{129}Xe gas was ready to be released into the sample container.

The samples investigated were freshly extracted human blood, plasma, hemoglobin solution, lysed red blood cell membranes (RBC ''ghosts'') in solution, and bovine serum albumin (BSA) solution. In each case, 25 ml of liquid were placed in a 60 cc capacity plastic syringe, which served as a sample container. Approximately 0.5 cc of sodium heparin per 25 ml of blood was added to prevent clotting. The samples of blood derivatives were prepared as follows. Plasma samples were obtained by centrifuging blood. The hemoglobin and red blood cell ghost samples were extracted from fresh citrated (CDP) human blood by a standard washing and centrifuging procedure. The red blood cells were isolated by being suspended three times in a phosphate buffer solution of 150 m*M* NaCl and 5 m*M* $NaPO_4$ and then centrifuged. The cells were lysed by adding a hypotonic solution of 5 m*M* $NaPO_4$ at pH 8, and then resuspended. Finally, the sample was centrifuged, producing a supernatant hemoglobin solution and a thick mixture of ghosts and white blood cells below. The bovine serum albumin (BSA) solution was made by dissolving powdered BSA (Sigma Chemicals) in deionized water at a concentration of 5 mg/ml.

The samples were either oxygenated or partially deoxygenated. The oxygenated samples were produced by flushing a mixture of 95% O_2 and 5% CO_2 six times through the sample syringe. The partially deoxygenated samples were produced by flushing six times with 95% N_2 and 5% CO_2. The delay between blood withdrawal and the NMR measurements was less than 3 h for all the samples. The blood samples were measured at room temperature but kept on ice during the time between measurements. Because of the gas space created when the xenon was introduced, the oxygenation levels changed from the initially prepared values. Under *in vivo* conditions, the average normal arterial oxygen saturation level, $S(O_2)$, of the hemoglobin is 97.5% at a partial pressure of oxygen, $P(O_2)$, of 100 mm Hg; and the venous oxygen saturation level is 75% at a $P(O_2)$ of 40 mm Hg (*26*). Values for $S(O_2)$ and $P(O_2)$ for our samples were estimated using temperature-dependent oxygen dissociation curves, and in some cases were directly measured using a co-oximeter. The estimated values for these two parameters agreed well with the directly measured values. Thus, the hemoglobin in the deoxygenated blood was less saturated than normal venous blood, and the hemoglobin saturation level of the oxygenated blood sample was approximately the same as normal arterial blood. The partial pressure of oxygen in the deoxygenated case was much less than venous conditions, while the partial pressure in the oxygenated case approximated normal venous conditions. In the case of the oxygenated plasma sample, the higher final oxygen partial pressure was a result of some residual oxygen bubbles in the syringe before introduction of the xenon.

Polarized-^{129}Xe gas introduced into the sample container expanded the enclosed volume in the syringe to 58 cc. The gas-sample mixture was vigorously agitated; for all sample types, a fine foam was formed that appeared stable for more than 1 minute. This foam provided a very large surface area for interaction between the gas and the sample, allowing xenon gas to be dissolved quickly into the sample, and depolarized ^{129}Xe in the sample to be replenished by the gas reservoir. In our analysis, the blood/gas foam mixtures were treated as representative of xenon dissolved in bulk blood. This assumption is supported by our observation of similar NMR spectra from ^{129}Xe dissolved in bulk blood (from a measurement with thermally polarized ^{129}Xe and no foam) and ^{129}Xe dissolved in blood foam. After the series of experiments, samples of the blood used were checked under a microscope and it was verified that less than 5% of the red blood cells had hemolyzed.

Once the polarized-^{129}Xe gas was mixed with a sample, the syringe was placed in a solenoid RF coil at the center of the spectrometer. Two sets of experiments were performed corresponding to the initial conditions of either $G \gg B$ or $G \sim B$. The case $G \gg B$ was the natural initial condition in our experimental setup. The case $G \sim B$ was produced by greatly reducing the ^{129}Xe gas magnetization by a series of four 90° pulses, and field gradient crushers [following the saturation method in Ref. (*27*)] were applied immediately prior to the measurement of $G(t)$ and $B(t)$. In addition to providing a consistency check, the case $G \sim B$ offers the advantage of analyzing the simpler and higher signal-to-noise ratio gas resonance.

A series of small flip angle RF pulses read out the ^{129}Xe magnetization. Since the frequency of dissolved ^{129}Xe in our samples was $\sim$200 ppm downfield from the frequency of the ^{129}Xe gas, we increased the signal-to-noise ratio (SNR) by alternating the frequency of the transmitter and receiver between 0 and 207 ppm relative to the gas; that is, alternately

on resonance with the gaseous and dissolved ^{129}Xe signals. This technique allowed for a narrower detection bandwidth and better utilization of the spectrometer's dynamic range. The duration of the rectangular read pulses was 87 μs, calculated to minimize the RF excitation 207 ppm away. Thus, each RF pulse selectively excited only one ^{129}Xe phase, gas or dissolved, without disturbing the other. For each run of the experiment, with a particular xenon-sample mixture, a total of 64 free-induction decays were acquired, 32 FIDs each at the gas and dissolved phase frequencies. The interpulse delay was either 1 s or 2 s. Crusher field gradients were applied after each signal acquisition to destroy any residual transverse coherence.

Because the laser polarization technique produces a highly nonthermal, and thus nonrecoverable, ^{129}Xe spin polarization, RF pulses with small flip angles are necessary to interrogate but not destroy the ^{129}Xe magnetization. The RF pulse amplitudes were set to provide flip angles of $\sim$2.5° on the gas and $\sim$15° on the ^{129}Xe dissolved in the sample. The flip angle on the gas could be smaller than that on the dissolved phase because of the significantly larger ^{129}Xe magnetization in the gas. For the case $G \sim B$, the flip angles were set to $\sim$15° for both the gas and dissolved ^{129}Xe phases. These angles were calibrated by measuring the magnetization destruction from a fast series of pulses and crusher gradients on a laser-polarized ^{129}Xe gas sample in a coated glass container with a T_1 longer than 2 h.

RESULTS AND ANALYSIS

Typical NMR resonances observed for laser-polarized ^{129}Xe dissolved in foam mixtures of blood, hemoglobin solution, red blood cell ghosts, plasma, and bovine serum albumin are shown in Fig. 1. Two peaks, of about the same area, at 197 and 220 ppm were observed for the blood samples. One narrow resonance at 197 ppm was observed in the plasma. All frequencies are in ppm relative to the ^{129}Xe gas resonance frequency at 0 ppm, not shown in Fig. 1. We conclude that the 197 ppm resonance is ^{129}Xe dissolved in blood plasma, and the 220 ppm resonance is ^{129}Xe in red blood cells. Both ^{129}Xe blood resonances have broadened widths compared to the single-component plasma case, indicating exchange between the components, and/or bulk magnetic susceptibility effects. The ghost sample has only one peak at 200 ppm with a broad pedestal which is probably due to residual hemoglobin. The albumin solution has one peak at 192.5 ppm, shifted upfield from the plasma. Table 1 summarizes the measured linewidths and chemical shifts for all the samples.

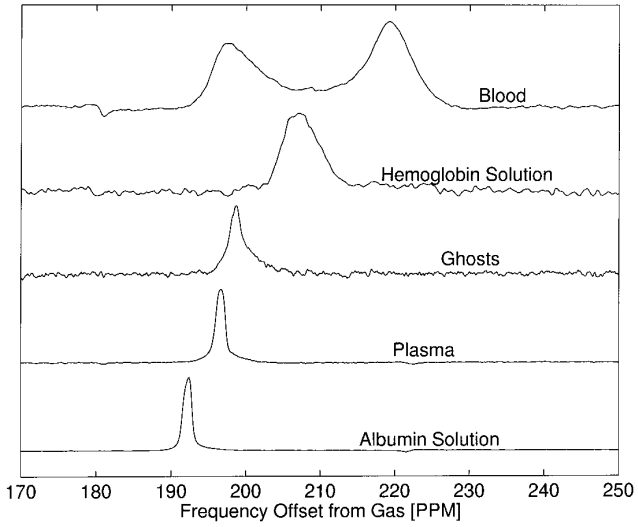

FIG. 1. NMR spectra of laser-polarized ^{129}Xe dissolved in foam preparations of blood, hemoglobin solution, red blood cell ghosts, plasma, and BSA. The small antiphase peak at $\sim$180 ppm in the blood spectrum is an artifact caused by the gas peak folding in.

TABLE 1
Summary of ^{129}Xe Linewidths and Chemical Shifts Relative to the Gas Peak

Sample	Oxygenation	Peak	Linewidth FWHM (Hz)	Chemical shift relative to gas (ppm)
Blood	Oxygenated	RBC	289 ± 12	220.0 ± 0.2
		Plasma	250 ± 22	196.7 ± 0.3
	Deoxygenated	RBC	336 ± 28	219.6 ± 0.3
		Plasma	292 ± 29	197.0 ± 0.4
Hb solution	Oxygenated		300 ± 90	208.8 ± 2.0
	Deoxygenated		305 ± 56	207.6 ± 1.1
RBC ghosts			157 ± 30	200.2 ± 0.4
Plasma	Oxygenated		72 ± 8	197.3 ± 0.1
	Deoxygenated		70 ± 11	196.8 ± 0.1
BSA			44.4 ± 2.6	192.5 ± 0.03

Note. The values given are the mean and standard deviation from eight consecutively acquired spectra.

The chemical shifts of the blood RBC and hemoglobin solution ^{129}Xe resonances differ from the previously measured value of 229.5 ppm for ^{129}Xe in hemoglobin (*28*), presumably because of fast exchange with the surrounding liquid. According to the solubility coefficients of xenon in red blood cells and plasma, 75% of the dissolved xenon in blood resides in the RBCs (*8*), with 45% of the total amount adsorbed on the hemoglobin (oxygenated or deoxygenated) (*22*). We infer that ^{129}Xe on the hemoglobin is in fast exchange with a subpopulation of the intracellular fluid, which in turn is in slower exchange (through the RBC membrane) with extracellular plasma. From the measured resonance linewidths, we estimate that the xenon exchange time between the RBC and plasma is $>$1 ms.

Figure 2 shows time-resolved-series spectra from the

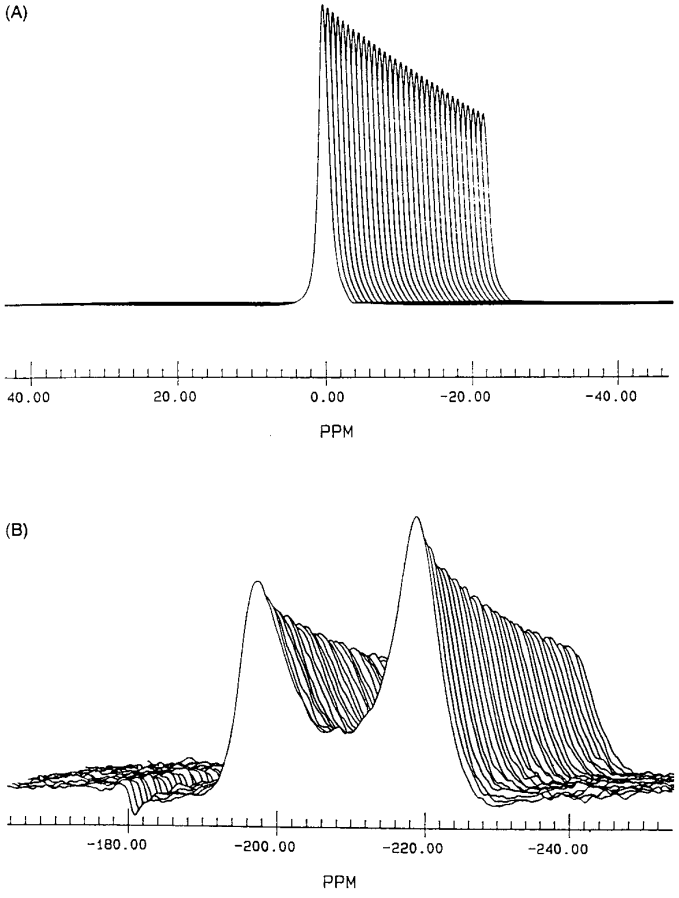

FIG. 2. Observed time series (2 s intervals) NMR spectra of laser-polarized ^{129}Xe dissolved in a sample containing oxygenated blood foam: (A) gas resonances and (B) blood resonances.

^{129}Xe gas phase and from ^{129}Xe dissolved in oxygenated blood, obtained at an offset from the gas spectra collection times. From such data, the various ^{129}Xe magnetization decay rates can be determined, as discussed above. Since the two ^{129}Xe blood resonances were observed to decay at the same rate, they were treated as one population. The first spectrum of each experimental run was phase corrected, with this phase correction fixed for the rest of the run. The ^{129}Xe peak areas were calculated for a fixed spectral width for each experimental run and were assumed to yield values proportional to the ^{129}Xe magnetizations in the blood and gas phases represented by $B(t)$ and $G(t)$, respectively.

The observed decay of the ^{129}Xe NMR peak integrals for blood, plasma, and gas phases for the initial conditions ($G \gg B$) are shown in Fig. 3. The observed gas decays for the case $G \gg B$ were monoexponential and were fitted with less than a 2% error in μ_2. The observed monoexponential behavior confirmed that, for $G \gg B$, the term $k_B B$ is negligible in the gas rate equation, Eq. [1]. The time behaviors of the integrals of the ^{129}Xe blood and plasma peaks were fitted using the Marquardt–Levenberg algorithm to a biexponential function (Eq. [4]) in which one of the decay rates was constrained to be the observed gas decay rate, μ_2. From such three-parameter fits, the second exponent, $\mu_1 = R_B - (\ln \cos \theta_B)/\tau + k_B$, was found. Table 2 summarizes the measured characteristic decay times corrected for the RF read pulses, $(\mu_1 + \ln \cos \theta_B/\tau)^{-1}$. These corrected decay times represent a lower limit on ^{129}Xe T_1 in the dissolved phase, see Eq. [8].

Similar measurements were performed for the initial condition $G \sim B$. This condition was obtained, as described earlier, by reducing the gas magnetization G with four 90° pulses applied immediately prior to the acquisitions. Figure 4 shows the ^{129}Xe blood, hemoglobin, and gas-phase peak integrals for the initial conditions $G \sim B$. For this condition, the dissolved phase-decay rate is best obtained from the gas-phase behavior due to the higher signal-to-noise ratio. The initial rise (0–10 s) of the gas signal and the fall of the blood/hemoglobin signal indicates ^{129}Xe magnetization

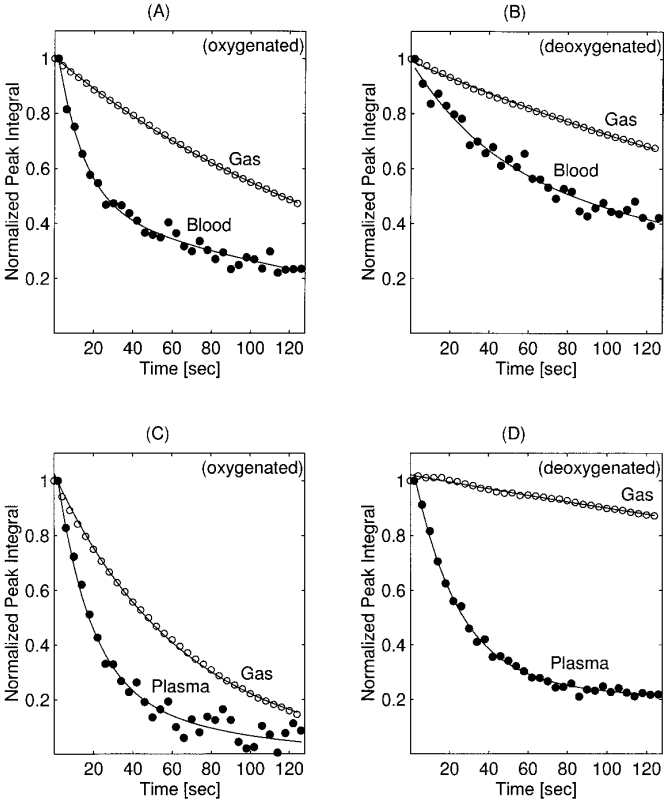

FIG. 3. Observed decay of NMR peak integrals for laser-polarized ^{129}Xe dissolved in (A) oxygenated blood foam, (B) deoxygenated blood foam, and (C) oxygenated and (D) deoxygenated plasma foam. Decay of the accompanying ^{129}Xe gas component (○) is shown above the blood and plasma signals (●). All ^{129}Xe integrals were normalized to the first point in the time series. In all cases, the gas-phase ^{129}Xe magnetization was much greater than the dissolved phase ^{129}Xe magnetization ($G \gg B$). The gas signals were fitted to monoexponentials, and the blood and plasma signals were fitted to biexponential functions (solid lines) with one exponential rate given by the observed gas signal decay rate.

TABLE 2
Summary of Measured ^{129}Xe Magnetization Relaxation Times for All Samples

(1) Sample	(2) O_2	(3) Initial conditions	(4) $P(O_2)$ (mm Hg)	(5) $S(O_2)$ (%)	(6) $\left(\mu_1 + \frac{\ln \cos \theta_B}{\tau}\right)^{-1}$ (s)	(7) Std. Dev. (s)	(8) T_1 (s)
Blood	Oxy	G ≫ B	40[a]	97[a]	17.6	+10.6/−4.8	17.6–22.9
		G ~ B	40.1	96.7	15.8	+5.2/−3.0	15.8–25.9
	Deox	G ≫ B	13[a]	58[a]	76	+∞/−42	>76
		G ~ B	12.9	58.1	40.6	+1.8/−1.6	>40.6
Plasma	Oxy	G ≫ B	50[a]	n/a	23.1	+8.4/−6.5	23.1–96.2
	Deox	G ≫ B	0[a]	n/a	30.4	2.5/−2.5	>30.4
Hb solution	Oxy	G ~ B	40[a]	96[a]	14.5	+4.1/−2.9	>14.5
	Deox	G ~ B	13[a]	58[a]	13.5	+0.9/−1.2	>13.5

Notes. Column (6) shows the lower limit of T_1; column (7) shows the calculated standard deviation error on the lower limit of T_1; column (8) shows the calculated range for T_1 from Eq. [8].

[a] Estimated values.

leaving the dissolved phase and entering the gas phase. In the blood samples, $(\mu_1 + \ln \cos \theta_B/\tau)^{-1}$ decreased upon oxygenation, consistent with results from the experiments where initially $G \gg B$ (see Table 2).

An additional, very early transient behavior (<4 s) is evident in the data with $G \sim B$ initial conditions (see Fig. 4). This indicates a rapid response to the large change in G induced by the 90° pulses. After pseudoequilibrium is destroyed by the 90° pulses, the ^{129}Xe polarization contained in the thin bubble walls of the blood/hemoglobin foam will quickly diffuse out of the liquid phase to reestablish a new pseudoequilibrium. Thus, the ^{129}Xe liquid-phase signal will drop suddenly and the ^{129}Xe gas signal will rise quickly. The behavior characterized by μ_1 will only be evident once the return to pseudoequilibrium is complete. For the case $G \gg B$, there is no such very early transient behavior because the system, during observation, is always in a pseudoequilibrium between G and B.

To illustrate the rapidity of ^{129}Xe exchange between the gas and liquid ^{129}Xe phases, and to examine the transient response to a large change in G, a 180° pulse was applied to the gas phase of a xenon–plasma system halfway through the polarization-decay time series. The pulses on each phase were chosen so as not to excite the other phase. Figure 5 shows the rapid change (~1 s) in the sign of the ^{129}Xe plasma peak after the 180° inversion pulse on the gas. This change in sign reflects, because of gas–plasma exchange, the magnetization inversion of the gas reservoir source.

The gas-phase xenon above each of the samples decayed differently in the presence of the four types of blood/plasma samples as can be seen in Fig. 3; that is, μ_2 differed for the four cases. This difference is probably due to the different partial pressures of gas-phase 0_2 which is paramagnetic and will cause ^{129}Xe depolarization (*29*). Nevertheless, for the sample type, different values of μ_2 led to the same extracted value for R_B. This was verified in several solutions by varying the flip angles or the pulse delays on the ^{129}Xe gas phase, thereby changing μ_2.

Our measurements suggest that ^{129}Xe retains its polarization for a significantly longer time in deoxygenated blood foam than in oxygenated blood foam. The measured characteristic decay times corrected for the RF pulses, $(\mu_1 + \ln \cos \theta_B/\tau)^{-1}$ are summarized in Table 2. Since the solubility of xenon does not depend on the partial pressure of oxygen (*22*), the values of k_B should be approximately the same for a given type of sample regardless of oxygenation. Hence, the comparison of the measured ^{129}Xe magnetization decay rates as a function of oxygenation should reflect the actual trend of T_1. The plasma samples also follow this trend. The measured decay times $(\mu_1 + \ln \cos \theta_B/\tau)^{-1}$ are lower limits to the intrinsic relaxation time T_1; the upper limit for T_1 is determined according to Eq. [8] with $\mu_{1(\text{low})}$ given by μ_1 found in the deoxygenated cases, assuming the exchange rates to be the same for a given sample, independent of oxygenation level. The calculated ranges for T_1 in the dissolved phase for each of the samples are listed in Table 2.

DISCUSSION

Oxygenation levels do not significantly affect the ^{1}H T_1 in blood or plasma, and when red blood cells are lysed, ^{1}H T_1 in the solution increases with oxygenation (*30, 31*). Thus, it may be surprising that the measurements reported here indicate that the ^{129}Xe blood T_1 decreases with oxygenation. This T_1 trend with oxygenation may be due to motion past paramagnetic sites created by O_2 dissolved in the aqueous

solution, a depolarizing effect much like that of O_2 on ^{129}Xe in the gaseous state (*29*). This trend may be more pronounced for ^{129}Xe than for ^{1}H due to the much shorter typical ^{1}H T_1 which may mask any oxygenation effect. Deoxygenated hemoglobin also creates paramagnetic sites (*32*), which may compete with the paramagnetic oxygen sites in solution in determining the T_1 trend with oxygenation. The absence of an oxygenation T_1 trend in the hemoglobin solutions may be due to a balance between these effects, or to the long times spent in the nonpolar binding sites of ^{129}Xe on hemoglobin. The reduced xenon and hemoglobin mobility in intact RBC compared to lysed cell solutions may create a subpopulation (intracellular) with a weak oxygenation dependence in exchange with a subpopulation in the plasma with a stronger oxygenation dependence. These possibilities require further study.

Exchange and oxygenation are two major issues to be considered when comparing the results reported here with previous work. Earlier *in vitro* measurements of the T_1 of polarized ^{129}Xe dissolved in blood found an oxygenation-T_1 trend opposite to that reported here. However, these preliminary measurements did not adequately account for gas–liquid exchange (*33*). Other experiments (*in vivo* and *in vitro*) (*12, 13, 15, 19*) reported only effective T_1 values because the measurements had xenon and oxygen exchange between dissolved and gas phases. From these measurements, the effective T_1 of resonances attributed to blood phase ^{129}Xe range from 5 to ~50 seconds. Also, no ^{129}Xe T_1 oxygenation trends were determined by these experiments. A thermal *in vitro* ^{129}Xe T_1 measurement (*6*) in a closed system found different T_1 values for plasma (10 s) and RBC (4.5 s), and no significant oxygenation trend. However, this experiment required several hours of acquisition time during which the $P(O_2)$ is suspected to have changed, and the blood components to have sedimented and degraded. To avoid these uncertainties, the $P(O_2)$ and $S(O_2)$ in our closed system experiments were measured explicitly, and laser-polarized ^{129}Xe was used to allow rapid measurement and hence insignificant blood sedimentation and degradation.

Systematics that could affect our T_1 measurements include: (i) coarsening of the foam; and (ii) RBC depletion in the foam. Foam coarsening would reduce k_B and B during the measurement period, thereby causing our model to underestimate T_1. RBC depletion (and hence plasma enrichment) in the foam could cause the extracted T_1 to overestimate the T_1 of *in vivo* blood. However, no visual evidence of either foam coarsening or RBC depletion (as indicated by the color of the foam) was observed during our measurements; also the decay of G was well fitted by a monoexponential, implying time-independent exchange constants, and thus no foam coarsening.

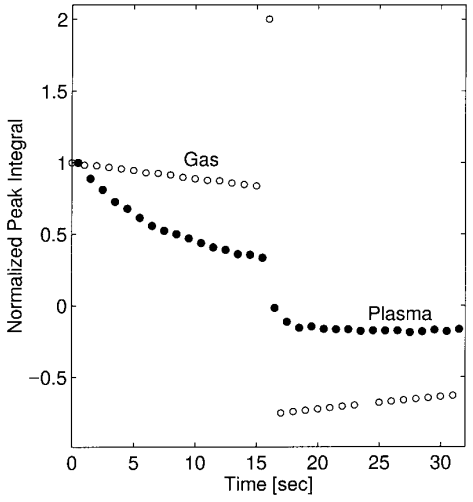

FIG. 5. Observed decay of signals from polarized ^{129}Xe gas and from ^{129}Xe dissolved in plasma. At t = 16 s, a 180° pulse is placed on the gas resonance. The plasma ^{129}Xe peak passed through zero and changed sign because of the plasma ^{129}Xe exchange with the inverted ^{129}Xe magnetization of the gas reservoir.

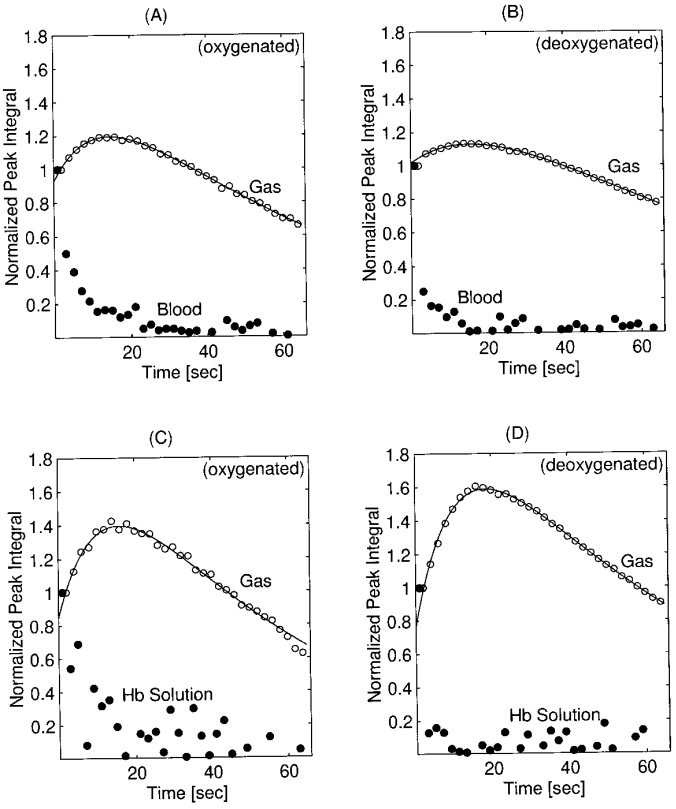

FIG. 4. Observed decay of NMR peak integrals for laser-polarized ^{129}Xe dissolved in (A) oxygenated blood foam, (B) deoxygenated blood foam, and (C) oxygenated and (D) deoxygenated hemoglobin foam. Decay of the accompanying ^{129}Xe gas component (○) is shown above the blood and plasma signals (●). The gas phase ^{129}Xe magnetization was greatly reduced by RF pulses prior to acquisition ($G \sim B$). The gas signals were fitted to biexponential functions (solid lines). All ^{129}Xe integrals were normalized to the first point in the time series.

The correspondence between the blood-foam system studied here and *in vivo* blood requires further study. Yet, it should be noted that generally *in vivo* measurements of the ^{129}Xe blood phase T_1 would be in an open system, and therefore would probably not be reliable. *In vitro* measurements can be made in closed systems, and thus allow the determination of a true T_1. Our *in vitro* measurements indicate that the ^{129}Xe blood T_1 decreases with increasing blood oxygenation in this experimental setup. Our measured values for ^{129}Xe blood T_1 were made with partial pressures of oxygen and hemoglobin oxygen saturation levels that differ from *in vivo* conditions. Nevertheless, if these results are extrapolated and applied to *in vivo* conditions, the ^{129}Xe T_1 is about 5 seconds, or roughly a lung–brain circulation time. This suggests that a significant amount of inhaled polarized ^{129}Xe could be transported to distal tissues such as the brain. The measurement technique using a foam gas–liquid exchange interface may also be useful for studying foam coarsening and other liquid physical properties (*34*).

ACKNOWLEDGMENTS

We are indebted to Robert Mulkern for valuable discussions and suggestions. We thank Joanne Ingwall for use of her laboratory resources; Kurt Saupe, Mattias Spindler, and Jeff Odiet for donation of blood; and John Bothwell for assistance in data analysis. We are grateful for contributions to the laser polarization technique provided by Glenn Wong. We also thank Samuel Patz and Daniel Williamson for useful comments, and Kathryn John and Tom Hoock for preparation of the hemoglobin samples. This work was supported by the NIH, the Burch Foundation, the Smithsonian Institution, the AFOSR, NASA, and the Whitaker Foundation.

REFERENCES

1. W. Happer, E. Miron, S. Schaefer, D. Schreiber, W. A. van Wijngaarden, and X. Zeng, *Phys. Rev. A* **29,** 3092–3110 (1984).
2. F. D. Colgrove, L. D. Schearer, and G. K. Walters, *Phys. Rev.* **132,** 2561–2572 (1963).
3. G. Eckert, W. Heil, M. Meyerhoff, E. W. Otten, R. Surkau, M. Werner, M. Leduc, P. J. Nacher, and L. D. Schearer, *Nucl. Instr. Meth. A* **320,** 53–65 (1992).
4. T. E. Chupp, R. J. Hoare, R. L. Walsworth, and B. Wu, *Phys. Rev. Lett.* **72,** 2363–2366 (1994).
5. M. E. Wagshul and T. E. Chupp, *Phys. Rev. A* **49,** 3854–3869 (1994).
6. M. S. Albert, G. D. Cates, B. Driehuys, W. Happer, B. Saam, C. S. Springer, Jr., and A. Wishnia, *Nature* **370,** 199–201 (1994).
7. M. Gatzke, G. D. Cates, B. Driehuys, D. Fox, W. Happer, and B. Saam, *Phys. Rev. Lett.* **70,** 690–693 (1993).
8. R. Y. Z. Chen, F-C. Fan, S. Kim, K-M. Jan, S. Usami, and S. Chien, *J. Appl. Physiol.* **49,** 178–183 (1980).
9. B. Driehuys, *Optics News,* **Dec,** 38 (1995).
10. H. Middleton, R. D. Black, B. Saam, G. D. Cates, G. P. Cofer, R. Guenther, W. Happer, L. W. Hedlund, G. A. Johnson, K. Juvan, and J. Swartz, *Magn. Reson. Med.* **33,** 271–275 (1995).
11. P. Bachert, L. R. Schad, M. Bock, M. V. Knopp, M. Ebert, T. Großmann, W. Heil, D. Hofmann, R. Surkau, and E. W. Otten, *Magn. Reson. Med.* **36,** 192–196 (1996).
12. K. Sakai, A. M. Bilek, E. Oteiza, R. L. Walsworth, D. Balamore, F. A. Jolesz, and M. S. Albert, *J. Magn. Reson. B* **111,** 300–304 (1996).
13. M. E. Wagshul, T. M. Button, H. F. Li, Z. Liang, C. S. Springer, K. Zhong, and A. Wishnia, *Magn. Reson. Med.* **36,** 183–191 (1996).
14. G. D. Cates, C. Charles, R. Black, B. Driehuys, W. Happer, A. Johnson, J. Macfall, H. Middleton, C. Ravin, B. Saam, K. Sauer, J. Swartz, M. Wagshul, and A. Wishnia, *Bull. Am. Phys. Soc.* **41,** 1104 (1996).
15. M. Rosen, K. P. Coulter, T. E. Chupp, S. D. Swanson, and B. W. Agranoff, *Bull. Am. Phys. Soc.* **41,** 1085 (1996).
16. S. D. Swanson, M. S. Rosen, K. P. Coulter, R. C. Welsh, and T. E. Chupp, Abstracts of the International Society of Magnetic Resonance in Medicine, 4th Annual Meeting, New York, p. 1360, 1996.
17. S. Peled, F. A. Jolesz, C-H. Tseng, L. Nascimben, M. S. Albert, and R. L. Walsworth, *Magn. Reson. Med.* **36,** 340–344 (1996).
18. M. S. Albert, V. D. Schepkin, and T. F. Budinger, *J. Comput. Assist. Tomogr.* **19**(6), 975–978 (1995).
19. A. Bifone, Y. Q. Song, R. Seydoux, R. E. Taylor, B. M. Goodson, T. Pietrass, T. Budinger, G. Navon, and A. Pines, *Proc. Natl. Acad. Sci. U.S.A.* **93,** 12,932–12,936 (1996).
20. S. Peled, C-H. Tseng, L. Nascimben, R. L. Walsworth, and F. A. Jolesz, Abstracts of the Experimental NMR Conference, 37th Annual Meeting, Pacific Grove, CA, p. 375, 1995.
21. J. R. Zimmerman and W. E. Brittin, *J. Phys. Chem.* **61,** 1328–1333 (1957).
22. B. P. Shoenborn, *Nature* **208,** 760 (1965).
23. G. D. Cates, R. J. Fitzgerald, A. S. Barton, P. Bogorad, M. Gatzke, N. R. Newbury, and B. Saam, *Phys. Rev. A* **45,** 4631–4639 (1992).
24. A. Kastler, *J. Phys. Radium* **11,** 255 (1950).
25. M. A. Bouchiat, T. R. Carver, and C. M. Varnum, *Phys. Rev. Lett.* **5,** 373–377 (1960).
26. J. B. West, ''Respiratory Physiology—The Essentials,'' 5th ed., Williams & Wilkins, Baltimore, 1995.
27. M. Pfeffer and O. Lutz, *J. Magn. Reson.* **108,** 106–109 (1994).
28. R. Tilton and I. Kuntz Jr., *Biochemistry* **21,** 6850–6857 (1982).
29. C. J. Jameson, A. K. Jameson, and J. K. Hwang, *J. Chem. Phys.* **89,** 4074–4081 (1988).
30. J. Gomori, R. Grossman, C. Yu-Ip, and T. Asakura, *J. Comput. Assist. Tomogr.* **11**(4), 684–690 (1987).
31. M-E. Meyer, O. Yu, B. Eclancher, D. Grucker, and J. Chambron, *Magn. Reson. Med.* **34,** 234–241 (1995).
32. L. Pauling and C. D. Coryell, *Proc. Natl. Acad. Sci. U.S.A.* **22,** 210–216 (1936).
33. M. S. Albert, D. Balamore, K. Sakai, D. Kacher, R. L. Walsworth, E. Oteiza, and F. A. Jolesz, Abstracts of the International Society of Magnetic Resonance in Medicine, ISMRM 4th Annual Meeting, New York, p. 1357, 1996.
34. C. P. Gonatas, J. S. Leigh, and A. G. Yodh, *Phys. Rev. Lett.* **75,** 573–576 (1995).